Proceedings of the ASME 2013 32nd International Conference on Ocean, Offshore and Arctic Engineering
OMAE2013
June 9-14, 2013, Nantes, France

OMAE2013-10285

Time Domain Analysis Approach for Riser Vortex-Induced Vibration Based on Forced Vibration Test Data

Kunpeng Wang, Wenyong Tang, Hongxiang Xue
State Key Laboratory of Ocean Engineering, Shanghai Jiao Tong University
Shanghai, China

ABSTRACT

As oil and gas exploration and production are pushed into deepwater area, the offshore industry is facing more challenges for riser vortex induces vibration (VIV). Although frequency domain approach has been widely used for the riser VIV prediction and fatigue design, several assumptions need to be made. In addition, frequency domain approach cannot account for the variable current and riser nonlinear boundary conditions, such as top boundary response, the interaction between riser and guides in the hull and soil-SCR interaction.

Considering above cases, several time domain codes have been developed for riser cross-flow (CF) VIV prediction. This paper presents a time domain approach based on forced algorithm. The exciting force is derived from the non-dimensional amplitude and frequency dependent lift coefficients from forced vibration test. The hydrodynamic damping model consists of empirical model and the extension of the lift curves. At each step, the displacement and velocity of each element would be obtained to calculate the response amplitude and frequency for the lift coefficient and damping. Expect for CF VIV, the mean drag force is also considered, which would be magnified by CF VIV.

The model test at Delta Flume of Delft Hydraulics is simulated using the proposed approach, and the CF VIV responses and the mean drag displacement are predicted. The results match well with the measured data.

INTRODUCTION

A riser is a key component of the oil and gas exploration and production system. When the current cross a riser, vortex will shed harmonically at the two sides and cause the riser vibration, namely vortex induced vibration (VIV). If the vortex shedding frequency is close to that of riser vibration, lock-in may happen and response amplitude can increase obviously, causing fatigue damage. Nowadays several frequency domain codes have been developed and successfully used for riser VIV prediction and fatigue damage design by making some conservative consumptions (Cheng, 2007), such as Shear7 (Vandiver et al., 2005) and VIVANA (Larsen et al., 2005). Frequency domain approach is efficient to achieve the parametric study. However, it cannot account for the current variation, the interaction between riser and guides in the hull and the SCR-soil interaction.

Although field test is effective to predict riser VIV, it is unfeasible due to high cost. Considering above cases, many researchers is engaged to develop time domain codes. Finn et al. (1999) and Grant et al. (2000) developed a time domain code ABAVIV to simulate riser VIV using the finite element package ABAQUS. In the code, the lock-in algorithm is proposed by Blevins (1990). Cheng el at. (2006, 2007, 2010) carried out lots of validation works for the code. The results shows that ABAVIV can well predict riser CF VIV and capture higher harmonics response, whereas lack ability to simulate mean drag response and in-line (IL) VIV. Sidarta et al. (2010) developed a SimVIV for time domain VIV prediction using the same algorithm with ABAVIV. As a new feature, SimVIV can predict riser IL VIV by simply assigning two times Strouhal frequency to IL response.

This paper presents a time domain approach for riser CF VIV using forced vibration test data by Gopalkrishnan (1993) at MIT. Outside the range of test data, empirical damping model proposed by Venugopal (1996) is used. The hydrodynamic coefficient is non-dimensional amplitude and frequency dependent. Therefore, at each step, the displacement and velocity of each element should be obtained to calculate the amplitude and frequency. In the excitation region defined in the following content, it is assumed that the response frequency is locked in the natural frequency nearest to the frequency associated with the non-dimensional frequency of 0.17 corresponding to the maximum hydrodynamic force, see Figure 2. Outside the excitation region, the calculated frequency is considered as the dominant frequency. Mean drag response coupled with CF VIV is an added feature in the study as the preparation for the IL VIV prediction. The model test at Delta Flume of Delft Hydraulics (Chaplin, 2005) is used for the validation of the present approach. The results show good agrement with the test data.

IL VIV prediction is not included in this paper. The next work will be engaged to the coupled analysis of CF VIV, IL VIV and mean drag response**.**

METHODOLOGY

MODEL FORMULATION

Deepwater riser is a kind of nonlinear slender structure. In the FEM analysis, it is usually divided into a finite number of discrete elements. A short element of riser is shown in Figure 1. The governing equilibrium equation could be expressed as:

CF direction:

$$m\frac{\partial^2 y}{\partial t^2}+c\frac{\partial y}{\partial t}+EI\frac{\partial^4 y}{\partial z^4}-\frac{\partial}{\partial z}\left(T\frac{\partial y}{\partial z}\right)=F_y\left(A_{CF}^*,f_{r,CF}\right) \tag{1}$$

IL direction:

$$m\frac{\partial^2 x}{\partial t^2}+c\frac{\partial x}{\partial t}+EI\frac{\partial^4 x}{\partial z^4}-\frac{\partial}{\partial z}\left(T\frac{\partial x}{\partial z}\right)=F_x\left(A_{CF}^*\right) \tag{2}$$

Where m is the riser mass per unit length, c the structural damping, E the elastic modulus, I the moment of inertia, T the effective tension, $F_x\left(A_{CF}^*\right)$ and $F_y\left(A_{CF}^*,f_{r,CF}\right)$ the mean drag force and hydrodynamic force in CF direction respectively, A_{CF}^* the ratio of CF amplitude A_{CF} to riser diameter D, $f_{r,CF}=f_{CF}D/V$ the dominant non-dimensional frequency, f_{CF} the dominant frequency of the riser response determined as followings, V the current velocity.

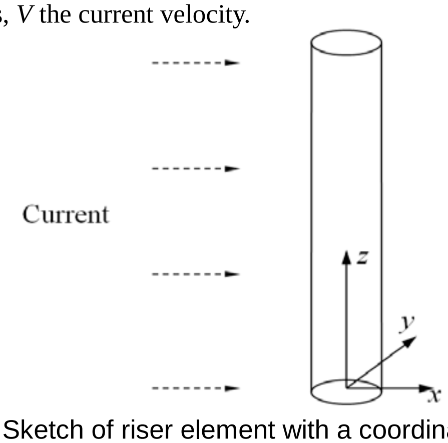

Figure 1. Sketch of riser element with a coordinate system

In the CF direction, the hydrodynamic force is decomposed into one component in phase with riser velocity, excitation force F_V, and one component in phase with riser acceleration, inertia force F_M. They are defined as:

$$\begin{aligned}F_V&=\frac{1}{2}C_V\left(A_{CF}^*,f_{r,CF}\right)\rho_f DV^2\cos(t)\\ F_M&=\frac{\pi}{4}C_M\left(A_{CF}^*,f_{r,CF}\right)\rho_f D^2\omega^2 A_{CF}\sin(t)=-m_{a,CF}\frac{\partial^2 y}{\partial t^2}\end{aligned} \tag{3}$$

where C_V and C_M is excitation coefficient and added mass coefficient, ρ_f fluid density, $\omega=2\pi f_{CF}$ dominant circular frequency, $m_{a,CF}$ added mass. In the present study, the C_M is set to 1.0.

Gopalkrishnan (1993) gave the contour of C_V as function of A_{CF}^* and $f_{r,CF}$, see Figure 2, where the thick line marks the important boundary between energy in and out. Positive excitation coefficient denotes that the excitation force synchronizes to the riser velocity, while negative excitation coefficient means damping. The associated damping coefficient is given as:

$$c_f=-\frac{C_V\rho_f V^2 D}{2A_{CF}\omega} \tag{4}$$

When (A_{CF}^* , $f_{r,CF}$) is out of the test data range, an empirical damping model proposed by Venugopal (1996) as well as the negative lift coefficient is employed to simulate the hydrodynamic damping. The damping model depends on the local non-dimensional frequency and is different for the high and low non-dimensional frequency regions.

High non-dimensional frequency damping model:

$$c_f=C_{lf}\rho_f DV+c_{sw} \tag{5}$$

where C_{lf} is an empirical coefficient taken to be 0.18. c_{sw} is the still water contribution given by:

$$c_{sw}=\frac{\omega\pi\rho_f D^2}{2}\left[2\sqrt{\frac{2}{\omega D^2/\nu}}+C_{sw}\left(\frac{A_{CF}}{D}\right)^2\right] \tag{6}$$

where ν is the kinematic viscosity of the fluid, C_{sw} an empirical coefficient taken to be 0.2.

Low non-dimensional frequency damping model:

$$c_f=C_{hf}\rho_f V^2/\omega \tag{7}$$

where C_{hf} is an empirical coefficient taken to be 0.2.

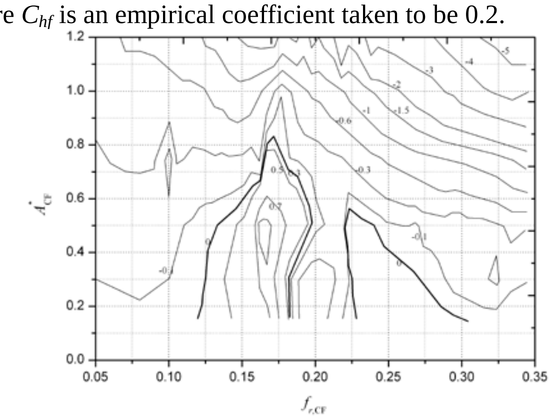

Figure 2. Contour plot of the excitation coefficient C_V (Gopalkrishnan, 1993)

In the IL direction, only mean drag force is considered, which is expressed as:

$$F_x\left(A_{CF}^*\right)=\frac{1}{2}C_D\rho_f DV^2 \tag{8}$$

where C_D is mean drag coefficient. Sarpkaya (1978) found that the mean drag coefficient has the following relationship with CF VIV amplitude:

$$\frac{C_D}{C_{D0}}=1+2A_{CF}^* \tag{9}$$

where C_{D0} is the mean value of the drag coefficient for a stationary cylinder.

DETERMINATION OF LOCK-IN REGIME

As with VIVANA (Larsen et al., 2005), the non-dimensional frequency with a range of [0.125, 0.20] is selected to determine the excitation region, which should be corrected for variations of Strouhal number. For an element of a riser, there may be many non-dimensional frequencies associated with different natural frequencies falling in the excitation region. At the initial calculation, the closer to the frequency associated with non-dimensional frequency of 0.17 corresponding to the maximum excitation coefficient is assumed to be the lock-in frequency and dominate the riser element response. After several cycles, the non-dimensional frequency associated with the calculated frequency will be judged whether it is in the excitation region. If yes, the closer natural frequency is still attached with the riser element as lock-in frequency, while if not, the calculated frequency will be used, and the element will be subjected to damping force. In this study, the attached frequency is referred to as the dominant frequency.

At the beginning, all riser elements are assigned to uniform amplitude, and then the amplitude and frequency can be calculated at each step through the obtained displacement and time at the adjacent two points with velocity of zero. Based on the obtained amplitude and dominant frequency, the hydrodynamic force is calculated, and translated to the next step for the VIV analysis. The flowchart of the analysis is illustrated in Figure 3.

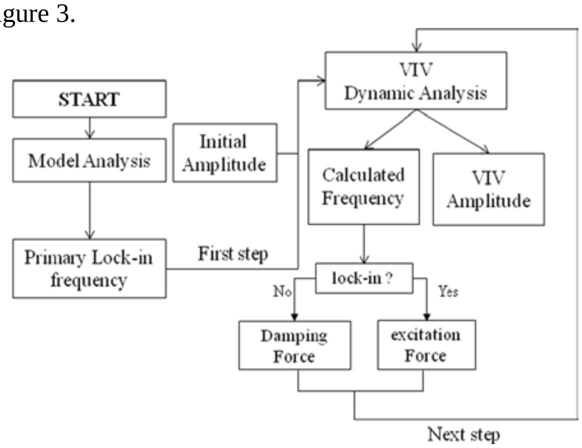

Figure 3. Flowchart of VIV analysis

VALIDATION AGAINST LABORATORY TEST

A model test for riser VIV was carried out by Chaplin (2005) in the flume tank at Delft Hydraulics Laboratory. Figure 4 gives the experimental system configuration. The 45% lower part of the riser was in the flume subjected to uniform current when the carriage moves with speed varying from 0.16 to 0.95m/s, while the upper part is in the still water. The properties of the riser are shown in Table 1. At the top, the riser was suspended with a set of springs whose pretension can be changed to simulate different riser tension.

In the test, 9 cases with varying tension and current were carried out and discussed. In this study, the present approach predicts four cases covering low and high current velocities, see Table 2. The FE model consists of 264 beam elements. The riser lower end boundary was simplified as fixed constraint, while the upper end was constrained in the horizontal degrees of freedom, and tensioned in the vertical direction. The mean value of the drag coefficient for the stationary riser used in the test is 1.33 (Aronsen, 2007).

At the early several cycles, Uniform amplitude was assigned to each element to create an initial CF response, and then the amplitude would be updated according to the response. Figures 5 and 6 give the time history response of node 50 with 2.5m from the lower end of the riser for cases A and B. Figures 7 and 8 give the time history response of node 240 with 1.3m from the upper end of the riser for cases C and D. Due to only considering the mean drag force in the current direction, the IL displacement almost remains constant or slightly fluctuates depending on the CF VIV amplitude. Figures 9~12 illustrate the corresponding amplitude spectrum of CF response. It is noted that single mode dominates the CF VIV response in the step current.

Figures 13~16 give the displacement envelopes of CF VIV. It is seen that the riser CF responses are conservative compared with the test data for cases A and B, while for cases C and D, the envelopes obtained from test covers the numerically predicted envelopes. The envelopes variation shows that the numerically and experimentally obtained displacements are in good agreement, and also indicates that the dominant mode is in general the same for cases A, B and C. However, for case D, only upper zone shows good comparison.

Figures 17~20 illustrate the RMS values of CF curvatures along the riser. The test data shows high order variation for case A which the present approach fails to capture. This may be due to that the test includes IL VIV which has influence on the CF curvature by coincidence for this case. For case B, the present approach gives conservative RMS values, but slightly underestimates them for cases C and D. It should be noted that when the riser is subjected to higher current and top tension exciting higher mode, the present approach usually predict lower results than the test.

Predicting the mean drag displacement in time domain is a new attempt. The numerically and experimentally obtained results along the riser are shown in Figures 21~24. From Eq.9, it could be known that the CF response has magnification effect on the IL mean drag displacement, so the present approach gives conservative results for case 1 and 2 due to the larger CF envelopes than test data.

CONCLUSIONS

This paper proposes an approach in time domain to predict the riser CF VIV and IL mean drag displacement. The forced test data and empirical damping model are applied to calculate the hydrodynamic force. Dominant frequency for each element is updated at each step and depends on the natural frequency, Strouhal frequency and calculated frequency. As a new attempt, IL mean drag displacement magnified by CF response is calculated.

To validate the present approach, the Laboratory VIV test in Delta Flume of Delft Hydraulics (Chaplin, 2005) is used in this study. The comparisons indicate that the predicted results using the present approach are in general close to the experimental data, such as CF displacement envelopes, RMS curvatures and mean drag displacement along the riser.

In this study, IL VIV is not taken into account, but some valuable works are already made, and the next work will focus on the coupled analysis of CF and IL VIV.

ACKNOWLEDGMENTS

This paper is based on the projects supported by the National Nature Science Foundation of China (Grant No. 51009089) and the Specialized Research Fund for the Doctoral Program of Higher Education of China (Grant No. 20100073120017).

REFERENCES

[1] Cheng, Y.M., Lambrakos, K.F., 2007. Time Domain Riser VIV Predictions Compared to Field and Laboratory Test Data. Proceedings of the 26th International Conference on Offshore Mechanics and Arctic Engineering, San Diego, California, USA.

[2] Vandiver J.K., Lee L., 2005. User Guide for SHEAR7 Version 4.4. Massachusetts Institute of Technology, Cambridge, Massachusetts, USA.

[3] Larsen C.M., Vikestad K., 2005. VIVANA-Theory Manual Version 3.4. Norwegian Marine Technology Research Institute, Trondheim, Norway.

[4] Finn, L., Lambrakos, K., Maher, J., 1999. Time Domain Prediction of Riser VIV. 4th International Conference on Advances in Riser Technologies, Aberdeen.

[5] Grant, R., Litton, R. and Finn, L., 2000. Highly Compliant Rigid Risers: Filed Test Benchmarking a Time Domain VIV Algorithm. Offshore Technology Conference, Houston, Texas, USA.

[6] Blevins, R.D., 1990. Flow-Induced Vibration. Van Nostrand Reinhold, New York.

[7] Cheng, Y.M., Lambrakos, K.F. 2006. Time Domain Computation of Riser VIV From Vessel Motions. Proceedings of the 25th International Conference on Offshore Mechanics and Arctic Engineering, Hamburg, Germany.

[8] Cheng, Y.M., Lambrakos, K.F. 2010. Time Domain VIV Prediction for Top Tensioned Risers. Proceedings of the 29th International Conference on Offshore Mechanics and Arctic Engineering, Shanghai, China.

[9] Sidarta, D.E., Finn, L.D. and Maher, J., 2010. Time Domain FEA for Riser VIV Analysis. Proceedings of the 29th International Conference on Offshore Mechanics and Arctic Engineering, Shanghai, China.

[10] Gopalkrishnan, R., 1993. Vortex induced forces on oscillating bluff cylinders. Ph.D. Thesis, Department of Ocean Engineering, MIT, Cambridge, MA, USA.

[11] Venugopal, M., 1996. Damping and Response Prediction of a Flexible Cylinder in a Current. Ph.D. Thesis, Department of Ocean Engineering, MIT, Cambridge, MA, USA.

[12] Chaplin, J.R., Bearman, P.W. and Huarte, F.J.H., 2005. Laboratory measurements of vortex-indcued vibrations of a vertical tension riser in a stepped current. Journal of Fluid of Structural, Vol. (21), pp: 3-24

[13] Sarpkaya, T., 1978. Fluid forces on oscillating cylinders. ASCE Journal of waterway, Port, Coastal, and Ocean Division, Vol. 104, pp: 275-290.

[14] Aronson, K.H., Larsen, C.M., 2007. Hydrodynamic Coefficients for In-Line Vortex Induced Vibrations. Proceedings of the 26th International Conference on Offshore Mechanics and Arctic Engineering, San Diego, California, USA.

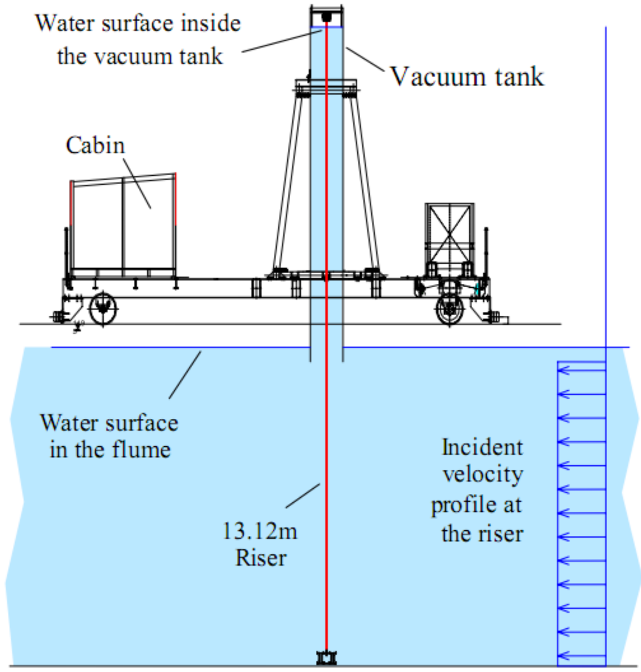

Figure 4. Delft Experimental Layout (Chaplin et al., 2005)

Table 1. Experimental riser properties at Delft

Parameters	value
Length	13.12 m
Diameter	0.028 m
Mass ratio	3.0
Submerged weight	12.1 N/m
In-Air weight	1.85kg/m
Bending stiffness (EI)	29.9 Nm^2
Axial stiffness (EA)	5.88 MN
Structural damping ratio	0.33%

Table 2. Test condition for VIV prediction

Cases	Current speed (m/s)	Top tension (N)
A	0.16	405
B	0.21	407
C	0.70	743
D	0.85	923

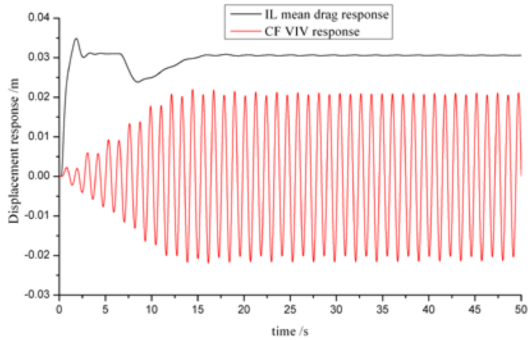

Figure 5. Riser response of Node 50 for case A

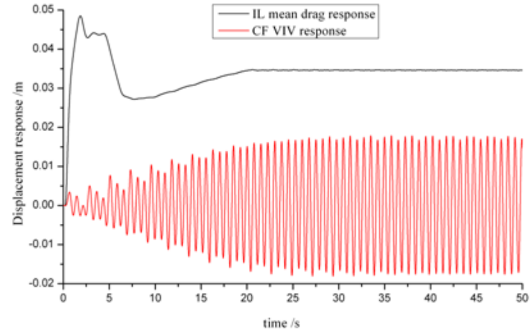

Figure 6. Riser response of Node 50 for case B

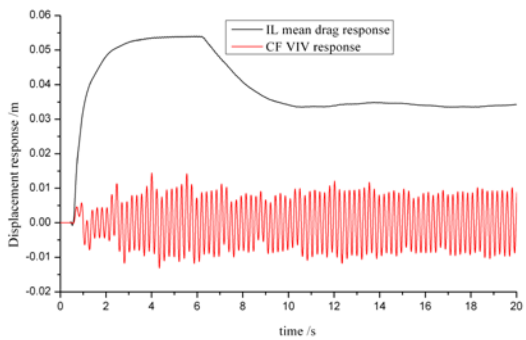

Figure 7. Riser response of Node 240 for case C

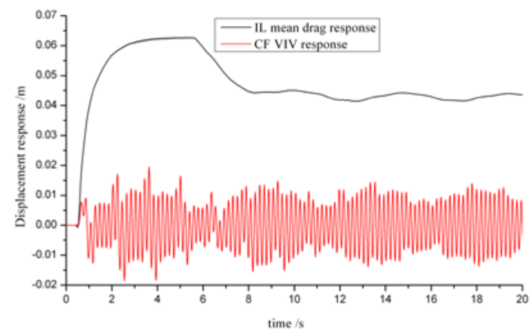

Figure 8. Riser response of Node 240 for case D

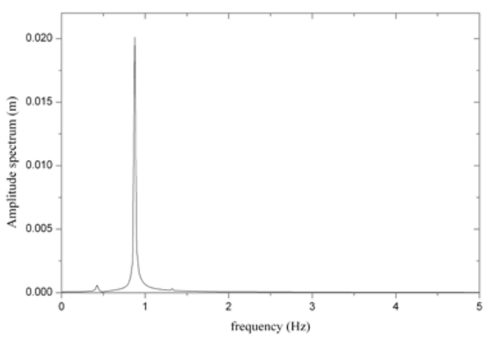

Figure 9. Amplitude spectrum of CF response at node 50 for case A

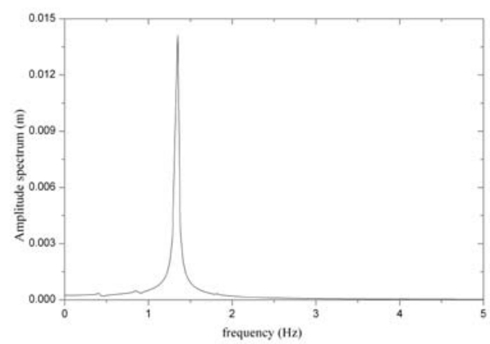

Figure 10. Amplitude spectrum of CF response at node 50 for case B

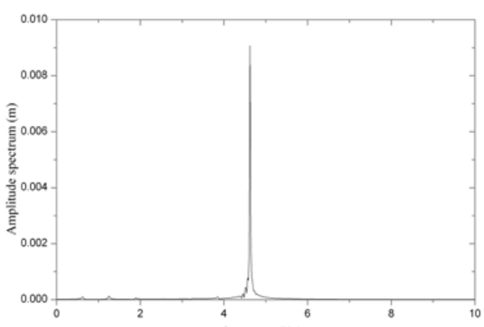

Figure 11. Amplitude spectrum of CF response at node 50 for case C

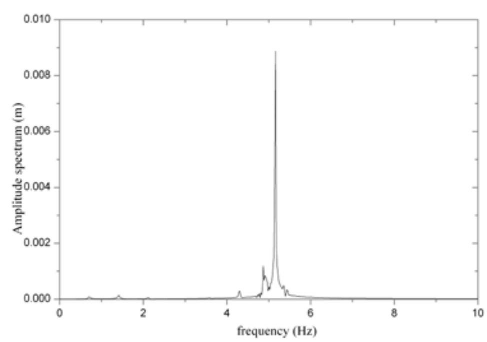

Figure 12. Amplitude spectrum of CF response at node 50 for case D

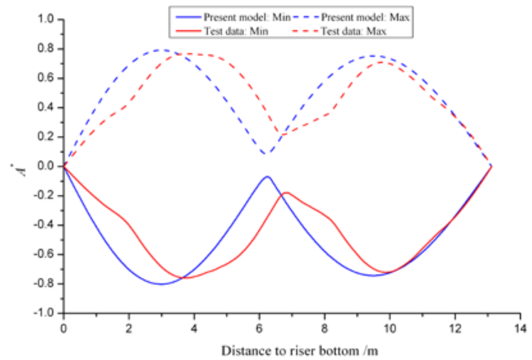

Figure 13. CF VIV displacement envelopes for case A

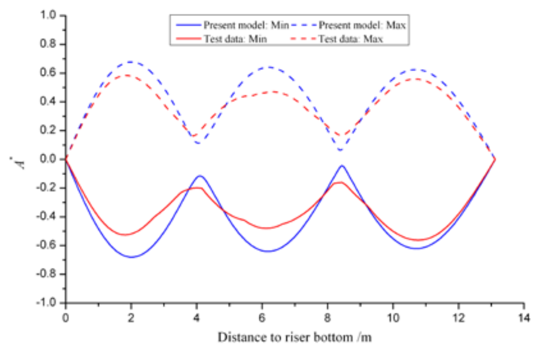

Figure 14. CF VIV displacement envelopes for case B

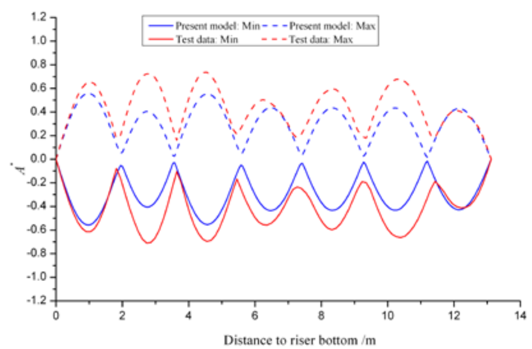

Figure 15. CF VIV displacement envelopes for case C

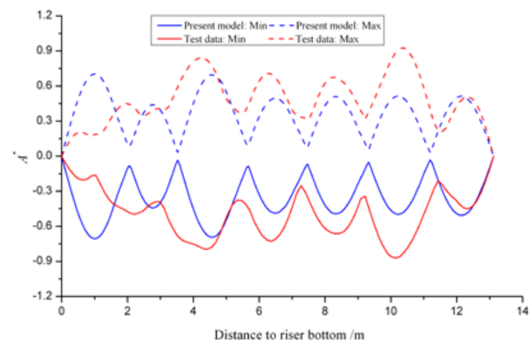

Figure 16. CF VIV displacement envelopes for case D

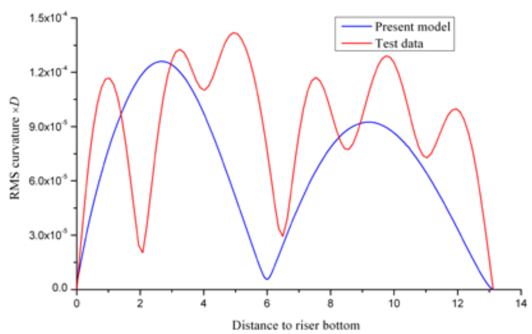

Figure 17. CF VIV RMS curvatures for case A

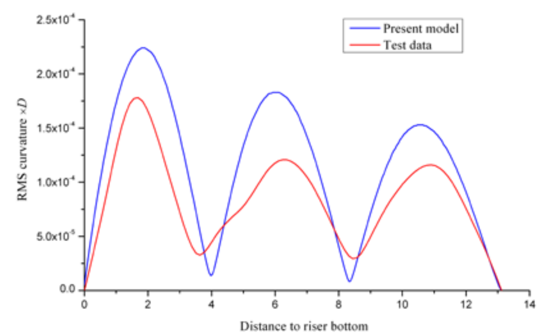

Figure 18. CF VIV RMS curvature for case B

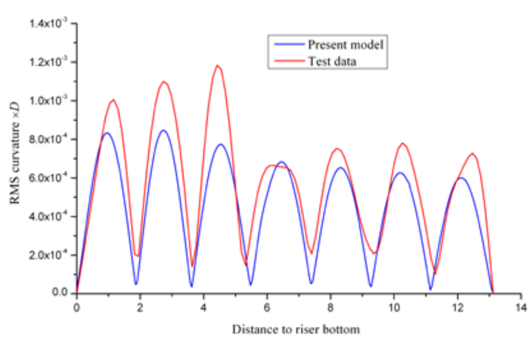

Figure 19. CF VIV RMS curvatures for case C

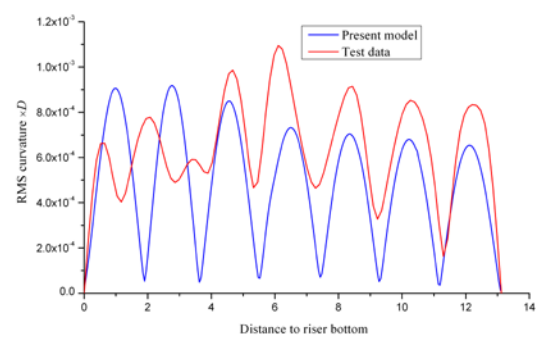

Figure 20. CF VIV RMS curvature for case D

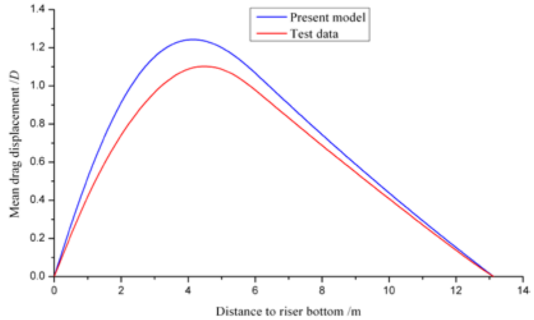

Figure 21. IL mean drag displacement for case A

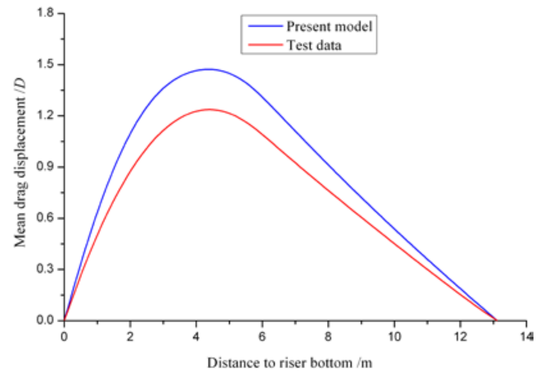

Figure 22. IL mean drag displacement for case B

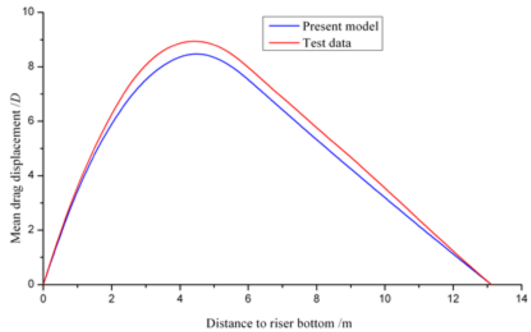

Figure 23. IL mean drag displacement for case C

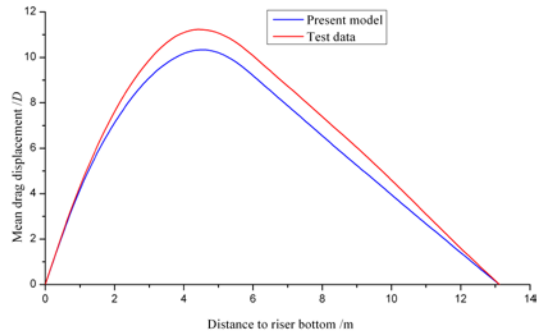

Figure 24. IL mean drag displacement for case D

